Combined Effects of Low-Dose Proton Radiation and Simulated Microgravity on the Mouse Retina and the Hematopoietic System

Authors: Mao, X. W., Boerma, M., Rodriguez, D., Campbell-Beachler, M., Jones, T., et al.

Combined Effects of Low-Dose Proton Radiation and Simulated Microgravity on the Mouse Retina and the Hematopoietic System

X. W. Mao,[a,1] M. Boerma,[c] D. Rodriguez,[a] M. Campbell-Beachler,[a] T. Jones,[a] S. Stanbouly,[a] V. Sridharan,[c] N. C. Nishiyama,[a] A. Wroe[b] and G. A. Nelson[a]

[a] *Departments of Basic Sciences, Division of Radiation Research and* [b] *Radiation Medicine, Loma Linda University School of Medicine and Medical Center, Loma Linda, California; and* [c] *Division of Radiation Health, Department of Pharmaceutical Sciences, University of Arkansas for Medical Sciences, Little Rock, Arkansas*

Mao, X. W., Boerma, M., Rodriguez, D., Campbell-Beachler, M., Jones, T., Stanbouly, S., Sridharan, V., Nishiyama, N. C., Wroe, A. and Nelson, G. A. Combined Effects of Low-Dose Proton Radiation and Simulated Microgravity on the Mouse Retina and the Hematopoietic System. *Radiat. Res.* **192**, 241–250 (2019).

The purpose of the current study was to characterize the effects of simulated microgravity and radiation-induced changes in retina and retinal vasculature, and to assess the accompanying early changes in immune cells and hematological parameters. To better understand the effects of spaceflight, we used a combination of treatments designed to simulate both the radiation and low-gravity aspects of space conditions. To simulate the broad energy spectrum of a large solar particle event (SPE) and galactic cosmic ray (GCR) radiation, male C57BL/6J mice were exposed to whole-body irradiation using fully modulated beams of 150-MeV protons containing particles of energy from 0 to 150 MeV and a uniform dose-vs.-depth profile. The mice were also hindlimb-unloaded (HLU) by tail suspension. Mice were unloaded for 7 days, exposed to 50 cGy, unloaded for an additional 7 days and then sacrificed for tissue isolation at days 4 and 30 after the combined treatments. Increases in the number of apoptotic cells were observed in the endothelial cells of mice that received radiation alone or with HLU compared to controls at both days 4 and 30 ($P < 0.05$). Endothelial nitric oxide synthase (eNOS) levels were significantly elevated in the retina after irradiation only or combined with HLU compared to controls at the 30-day time point ($P < 0.05$). The most robust changes were observed in the combination group, suggesting a synergistic response to radiation and unloading. For hematopoietic parameters, our analysis indicated the main effects for time and radiation at day 4 after treatments (day 11 postirradiation) ($P < 0.05$), but a smaller influence of HLU for both white blood cell and lymphocyte counts. The group treated with both radiation and HLU showed greater than 50% reduction in lymphocyte counts compared to controls. Radiation-dependent differences were also noted in specific lymphocyte subpopulations (T, B, natural killer cells). This study shows indications of an early effect of low-dose radiation and spaceflight conditions on retina and immune populations. © 2019 by Radiation Research Society

INTRODUCTION

Microgravity and radiation are stressors unique to the spaceflight environment, and can affect the central nervous system (CNS) and immune system. They could potentially lead to significant risks to astronaut health both acutely, during the course of a mission, or chronically, leading to long-term, post-mission decrements in quality of life. A recently published study showed that more than 50% of the astronauts returning from space have reported changes in their visual acuity (*1*). To date, the mechanisms behind these effects are not fully understood. Evidence also shows that exposure to space flight induces immune alterations in astronauts (*2*).

Studies have shown that both microgravity encountered by astronauts in space, as well as modeled microgravity on Earth, can induce many deleterious physiological effects, including changes in ocular structure and function (*3*). After long-duration spaceflight, morphological changes in the optic nerve and surrounding tissues have been reported (*4*). Microgravity induces a significant head-ward shift in body fluids and an increase of intraocular pressure (*5*). These changes within the CNS affect retinal structure and function (*6*). However, the cellular mechanisms of the unique physiological and pathological ocular responses are unknown. Microgravity-related immunological changes and immune dysregulation have also been reported. Exposure to microgravity or simulated microgravity also induces changes in the numbers of several types of immune cells in the circulation (*7, 8*).

The space radiation environment consists of highly charged and energetic particles that include high-energy protons in the galactic cosmic ray (GCR) spectrum and are released from the sun during solar particle events (SPEs).

[1] Address for correspondence: Loma Linda University, Basic Sciences, 11175 Campus St., Room A1010, Chan Shun Pavilion, Loma Linda, CA 92350; email: xmao@llu.edu.
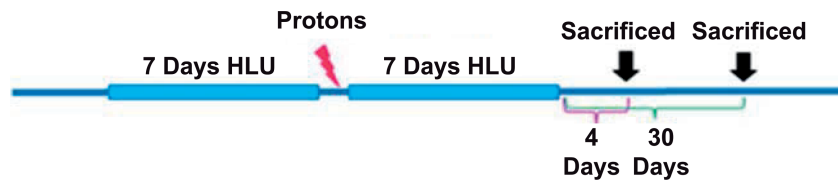
FIG. 1. Experimental protocol. Mice underwent hindlimb-unloading (HLU) for 7 days, received whole-body irradiation at a single dose of 50 cGy, then HLU for an additional 7 days and were then sacrificed for tissue isolation at days 4 and 30 after the combined treatments. Radiation was delivered as a fully modulated beam of 150 MeV protons to give a broad energy distribution similar to a solar particle event (SPE) and galactic cosmic ray (GCR) radiation spectrum.

During long-term deep space missions, it is anticipated that multiple SPEs will be encountered. Furthermore, an SPE dose may also exacerbate biological effects from the concurrent protracted GCR radiation exposure (*9*). These exposures are a significant radiation hazard to astronauts and spacecraft. Studies on mice that had been subjected to radiation and space flights (*10–14*) have shown that environmental conditions have profound effect on retinal endothelial health and retinal function. In a previously published study, we showed that a dose of 0.5 Gy proton radiation significantly induced oxidative stress-associated apoptosis in the retina (*10*). Cells of the immune system are also vulnerable to the effects of radiation (*15*). Many studies have demonstrated in rodent models that total-body irradiation with protons can induce immune depression and that some abnormalities persist long-term (*16–19*). Combined exposure to space radiation and hindlimb suspension has significantly affected the number of circulating blood cells (*20*) and reduced the ability to control bacterial challenge in a mouse model due to impaired immune function (*21*).

Oxidative stress-induced ocular tissue damage resulting from reactive oxygen species (ROS) has been associated with a variety of pathological and environmental conditions, including radiation. Accumulating evidence suggests that ROS interfere with nitric oxide (NO) regulation causing endothelial dysfunction (*22*). NO, which is derived from L-arginine in an oxidizing reaction catalyzed by NO synthase (NOS), serves multiple functions, including vasodilation, neurotransmission and immune defense (*23*). In mammalian cells, three distinct isoforms of NOS have been identified: neural NOS (nNOS), inducible NOS (iNOS) and endothelial NOS (eNOS). Among these isoforms, eNOS is the major source of NO production in endothelial cells (*24*). Our recently published study showed significant increased expression of eNOS immunoactivity in retinal endothelial cells after oxygen and proton irradiation compared to controls (*25*). This analysis indicated that heavy ion-charged particles may activate eNOS, promote apoptosis in retinal endothelial cells and contribute to endothelial dysfunction.

The purpose of the current study was to characterize early effects of combined hindlimb unloading (HLU) and radiation-induced changes in retina and retinal vasculature and assess the accompanying early changes in immune cells and hematological parameters. We hypothesized that simulated microgravity may enhance the effects of space-like radiation on retinal vascular endothelial cells, circulating blood cells and hematopoietic function.

MATERIALS AND METHODS

Animals

Six-month-old, male C57BL/6J mice, each weighing approximately 26–30 g, were purchased from the Jackson Laboratory (Bar Harbor, ME). Upon arrival, animals were housed in cages (cage size: 17 × 9 × 6 in) within a BioZone® VentiRack™ (BioZone Inc., Fort Mill, SC). Animals were maintained under a constant ambient temperature of 68°F with a 12:12 h light-dark schedule throughout the study. Commercial pellet chow, Lab Diet 5LG4 (Lab Diet, St. Louis, MO) and hydrogel (ClearH$_2$O®, Portland, ME) were available *ad libitum*. After acclimatization for approximately 7 days, the mice were housed one per cage and assigned to the following groups: 1. control; 2. whole-body proton irradiation; 3. HLU; 4. combined treatments. There were 8 mice/group. The study followed recommendations in the Guide for the Care and Use of Laboratory Animals of the National Institutes of Health and was approved by the Institutional Animal Care and Use Committee (IACUC) of Loma Linda University (Loma Linda, CA). The animals in the combined treatments group were HLU for 7 days, then received 50 cGy proton whole-body irradiation, followed by HLU for an additional 7 days and then sacrificed for tissue isolation at days 4 and 30 after the combined treatments (Fig. 1). After the HLU and irradiation period, mice were returned to group housing, four per cage, until euthanasia. At the appropriate time point, mice were deeply anesthetized with 3% isoflurane followed by immediate exsanguination via inferior vena cava (IVC) puncture. Animals' health status, food and water intakes were monitored on a daily basis.

Hind Limb Unloading

Hind limb unloading is a widely accepted, ground-based animal model that simulates the mechanical unloading and body fluid shifts encountered in microgravity (*26*). Such changes in fluid perfusion could contribute to increases in intracranial or intraocular pressure (*5*). The cage floor was made with a grid panel to allow for animal and food waste to fall through the cage. For suspension, the tail was inserted into a plastic tube of a tail harness and attached to a loop of tape at the tip of the tail, and to a swivel fixed on a guide-wire running the length of the cage. The height of the bar is adjusted to maintain the animal in a 35- to 40-degree head-down tilt with the hind legs elevated above the bottom of the cage. In this model, the forelimbs are used for locomotion and grooming. The control animals were not tail-suspended. Animals were observed daily for changes in appearance and activity.

Irradiation with Protons

The mice received either sham irradiation or 50 cGy protons whole-body irradiation (n = 8/group). The mice were restrained individually in 1.5-mm thick, rectangular plastic boxes (3 × 3 × 8.5 cm) with air holes. The proton beam was orientated vertically downward such that the mice were dorsally irradiated. SPE-like exposures were simulated using a fully modulated 149.6 MeV/nucleon proton beam. The full modulation of the monoenergetic proton beam was produced by passing it through a rotating propeller-like modulator wheel with 21 thickness steps machined into the blades to range shift the single incident proton energy into 21 separate proton energies. A 2.0-cm-thick plastic water range shifter was utilized in the irradiations to ensure dose uniformity over the entire animal. When the Plastic Water™ range shifter was combined with the 1.5-mm-thick mouse box wall, the lowest Bragg peak energy incident on the test subject was 24.6 MeV, while the highest was 122.5 MeV. The superposition of 21 Bragg peaks created a uniform dose region (known as the spread-out Bragg peak) across the entire animal regardless of its orientation within the holder. Nonirradiated controls (sham irradiation) were immobilized for the same length of time, positioned in the proton irradiation field without exposure.

Eye and Retina Preparation

At days 4 and 30 postirradiation with HLU, mice were euthanized and the right eye from each mouse was placed individually in a sterile cryovial, snap frozen in liquid nitrogen and kept at –80°C prior to use. The left eyes were fixed in 4% paraformaldehyde (PFA) in phosphate buffered saline (PBS) for immunohistochemistry (IHC) assays.

Immunostaining Assays and Histology

Six μm paraffin-embedded sections were cut through each eye; sections were approximately 100 μm apart, providing 10 sections per eye for analysis. To characterize apoptosis, 5 sections were subjected to terminal deoxynucleotidyl transferase dUTP nick end labeling (TUNEL) staining. Retinal tissues were evaluated using the Dead-End™ Fluorometric TUNEL system kit (Promega Inc., Madison, WI). Sections were then stained with DyLight® 488 *Lycopersicon esculantum*-Lectin (Vector® Laboratories, Burlingame, CA) for labeling vascular networks at a 1:100 dilution for 30 min at room temperature. Five tissue sections of each retina were examined using a BZ-X710 All-in-One inverted fluorescence microscope with structural illumination (Keyence Corp., Elmwood Park, NJ). TUNEL-positive cells were identified by green fluorescence, vascular endothelia were identified with red fluorescence; the nuclei of retinal cells were counterstained with diamidino-2-phenylindole (DAPI, blue). TUNEL-positive cells that were located within red lectin-labeled endothelium were identified as TUNEL-positive endothelial cells. To characterize eNOS function and associated oxidative damage in retina and retinal endothelial cells, five ocular sections from each eye were incubated with rabbit anti-eNOS primary antibody (Abcam®, Cambridge, UK) at 1:100 dilution at 37°C for 1 h, followed by a goat anti-rabbit IgG Dylight 594 secondary antibody (Thermo Scientific™, Hampton, NH) at 1:200 dilution for 1 h at room temperature.

Sections were then stained with DyLight 488-Lectin (Vector Laboratories) at a 1:100 dilution for 30 min at room temperature. eNOS activity was identified by green fluorescence; vascular endothelia were identified with red fluorescence and the nuclei of retinal cells were counterstained with DAPI (blue fluorescence). eNOS-positive cells that were located within red lectin-labeled endothelium were identified as eNOS-positive endothelial cells.

For quantitative analysis, the total number of TUNEL- or eNOS-positive cells in the retinal vessels were counted in five sections of each eye. The area of selected region was measured on digital microphotographs using ImageJ counting plugin 1.41 software (NIH, Bethesda, MD; http://rsbweb.nih.gov/ij/). The density profiles were expressed as mean number of apoptotic or eNOS-positive cells/mm². Similar procedures for density evaluation have been described elsewhere (*11, 25*). The mean of the density profile measurements across five retina sections per eye was used as a single experimental value.

Hematological Analysis in the Blood

At the time of euthanasia, blood was obtained through IVC puncture with ethylenediaminetetraacetic acid (EDTA)-containing syringes. A Vet ABC Hematology Analyzer (Scil Animal Care, Gurnee, IL) was used to obtain white blood cell (WBC), major leukocyte population (lymphocyte, monocyte, granulocyte), red blood cell (RBC), platelet (PLT) counts and mean platelet volume (MPV). Values for hemoglobin (HGB) concentration, hematocrit (HCT, proportion of blood volume composed of RBC), mean corpuscular volume (MCV, average RBC volume), mean corpuscular hemoglobin (MCH, average mass of HGB/RBC), mean corpuscular HGB concentration (MCHC, average HGB/RBC), RBC distribution width (RDW, width of RBC based on cell number × cell size) and mean platelet volume (MPV, average platelet size) were obtained. Granulocyte, monocyte and lymphocyte counts and percentages were also measured.

Spleen Processing and Leukocyte Analysis

Spleens were cut into thirds and weighed. One third of the organ was immediately frozen in liquid nitrogen for further analysis. Two thirds were placed into 1 ml RPMI 1640 medium (Mediatech Inc., Herndon, VA), homogenized using sterile wooden applicator sticks and filtered through 40-Pm nylon filters (BD Biosciences, San Jose, CA). Once in single-cell suspensions, splenocytes were counted with the ABC Analyzer, as described above. Leukocyte counts were corrected for the mass.

Flow Cytometry Analysis of Lymphocyte Subpopulations in Blood and Spleen

A two-tube custom-conjugate mixture with fluorescence-labeled monoclonal antibodies (mAb), a direct-staining procedure, was used to identify specific leukocyte types using a FACSCalibur™ flow cytometer (Becton, Dickinson and Co., San Jose, CA). The mAb were labeled with fluorescein isothiocyanate (FITC), R-phycoerythrin (PE), allophycocyanin (APC) or peridinin chlorophyll protein (PerCP). For lymphocyte phenotyping, a two-tube custom-conjugate mAb mixture (BD Biosciences, San Diego, CA) was used to identify CD3+ for mature T cells, CD19+ for B cells and NK1.1+ for natural killer (NK) cells. Analysis of 5,000–10,000 events/tube was performed using CellQuest™ software version 3.1 (Becton, Dickinson and Co.).The percentages obtained were used together with cell numbers from the hematology analyzer to obtain numerical data for each lymphocyte population.

Statistical Analysis

The results obtained from IHC evaluation were analyzed using one-way analysis of variance (ANOVA) followed by Tukey's post hoc multiple-comparison test (SigmaPlot™ for Windows, version 13.0; Systat® Software Inc., Point Richmond, CA). The significance level was set at $P < 0.05$. Data are shown as mean ± standard error (SEM).

The results obtained from hematological and splenocyte analysis were analyzed by three-way ANOVA to determine main effects and interaction using radiation, HLU and time points as the independent variables followed by Tukey's honestly significant difference post hoc multiple-comparison test. The significance level was set at $P < 0.05$. Data were shown as mean ± SEM. The terms ''main effect'' and ''interaction'' are common statistical terms used in describing ANOVA results. In our case, there were three independent variables:

Controls | **Irradiation**

HLU | **Combination**
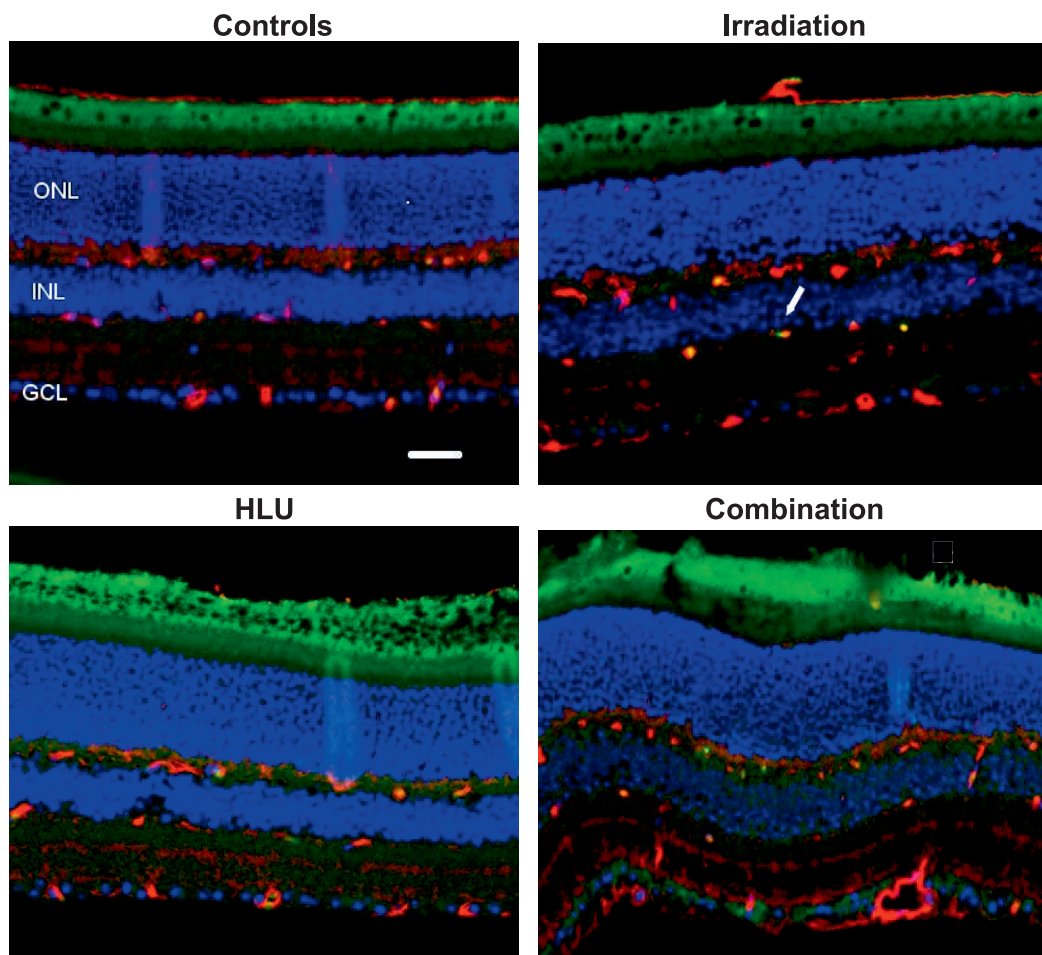
FIG. 2. Apoptosis based on TUNEL staining of retinal tissue. Panel A: Control; panel B: 50 cGy proton irradiation; panel C: hindlimb unloading (HLU); panel D: combined treatment. TUNEL-positive cells were identified with green fluorescence and endothelium was stained with lectin (red). The nuclei of photoreceptors were counterstained with DAPI (blue). TUNEL-positive cells that were located within red lectin-labeled endothelia were identified as TUNEL-positive endothelial cells. ONL = outer nuclear layer; INL = inner nuclear layer; GCL = ganglion cell layer. The arrow indicates TUNEL-positive endothelial cell. In the control retinal tissue, only sparse TUNEL-positive cells were found. In the retina of the combined treatments (50 cGy proton irradiation with HLU), TUNEL-positive labeling was apparent in the endothelial cells. Scale bar = 50 μm. Green autofluorescence was noted in the outer layers.

radiation, HLU and time. A significant main effect of radiation means that the effect of radiation was significant, independent of any effect of HLU or time. Similarly, a significant radiation × HLU interaction means that the effect of radiation was significantly dependent on the effect of the HLU.

RESULTS

Body Weights

Mean animal mass for each group prior to irradiation and/or HLU was as follows: control = 29.4 ± 0.6 g; irradiation only = 29.4 ± 0.9 g; HLU only = 28.9 ± 0.8 g; and combination = 28.2 ± 0.7 g. At sacrifice (day 4 postirradiation), masses were as follows: control = 31 ± 0.6 g; irradiation only = 29.7 ± 0.8 g; HLU only = 29.9 ± 0.5 g; and combination = 29.8 ± 0.5 g. At the one-month time point, masses were as follows: control = 31 ± 0.5g,

irradiation only = 31.5 ± 0.7 g, HLU only = 30.7 ± 1.0 g; and combination = 29.5 ± 1.1 g. There were no significant group differences in pre-exposure mass compared to mass at time of sacrifice.

Apoptosis in Retinal Endothelial Cells at Days 4 and 30 after Proton Irradiation and HLU

At day 4 postirradiation with HLU, an increase in TUNEL-positive cells was noted in the retinal inner nuclear layer (INL) after proton irradiation and in the combined treatments cohort (Fig. 2). Our quantitative assessment revealed that TUNEL-positive retinal endothelial cell density was the highest in the combination group at the 4-day time point ($P < 0.05$) compared to other groups. The counts for controls were significantly lower than all other groups at the 30-day time point ($P < 0.05$) (Fig. 3). The
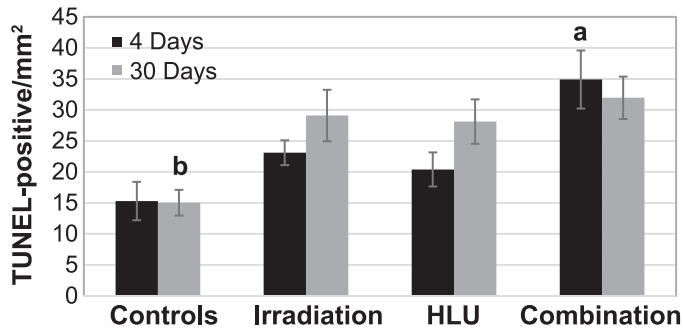
FIG. 3. Immunoreactivity of TUNEL staining in the retinal endothelium after irradiation and/or HLU. Values are presented as mean density ± SEM for 8 mice/group. "a" indicates significantly higher than all other groups at the 4-day time point ($P < 0.05$). "b" indicates significantly lower than all other groups at day 30 ($P < 0.05$).

most robust changes were observed in combined treatments groups compared to the control group.

eNOS Immunoreactivity in Retinal Endothelial Cells after Proton Irradiation and HLU

There were no significant differences among groups at day 4 for eNOS expression. However, by day 30, increased eNOS staining was seen in the retinal INL after the combined treatments of radiation and HLU (Fig. 4). Quantitative analysis revealed that eNOS immunoreactivity was significantly higher ($P < 0.05$) in the combined treatments group compared to control and irradiated-only groups at the 30-day time point (Fig. 5).

Blood and Spleen Analysis

There were significant main effects of radiation ($P < 0.05$) for WBC and lymphocyte counts in the blood (Fig.

6A). Our quantitative analysis showed significant interactions in WBC and lymphocyte counts between exposure and HLU at day 4 ($P < 0.05$), suggesting that unloading significantly augmented the response to radiation. Post hoc analysis showed that the WBC and lymphocyte counts were greatly reduced after irradiation at both days 4 and 30 with smaller influences of HLU on both total WBCs and lymphocytes. With the exception of day 30 for lymphocyte, the combined treatments group had consistently lower counts than other groups. The combined treatments group had over 50% lower lymphocyte counts compared to the control and HLU groups by day 4 ($P < 0.05$). For platelet counts, there were no significant differences among groups for both time points, except for the following: On day 4, the HLU group had significantly higher counts compared to controls ($P < 0.05$) and a strong trend increase compared to the combined treatments group ($P = 0.07$) (Fig. 7). There were no significant differences in RBC or other platelet measurements and time points among groups (data not shown).

Analysis of the spleen showed at day 4 that there were no significant main effects from radiation or HLU on the counts of any major immune cell subset (Fig. 6B). There was a significant interaction of radiation and HLU by day 30 for WBCs and lymphocytes ($P < 0.05$). The combined treatments group had the lowest counts. There were no significant differences in RBC and platelet measurements between groups (data not shown).

Major Lymphocyte Populations in Blood

Since lymphocytes are the most radiosensitive of all leukocyte subsets, we characterized T ($CD3^+$), B ($CD19^+$) and NK (NK1.1) cell subsets in the blood and spleen using flow cytometry. By day 4, there were significant main
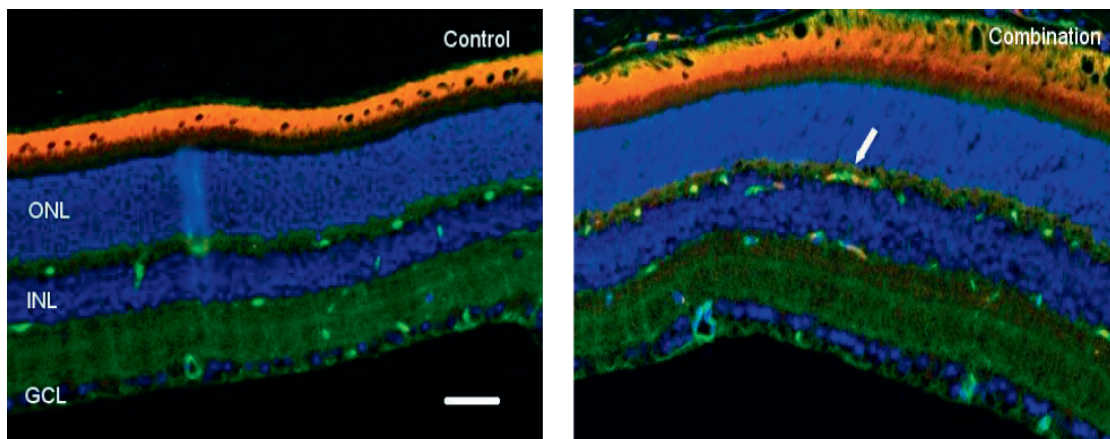
FIG. 4. Representative micrographs of retina sections evaluated for eNOS expression at day 30 after a dose of 50 cGy proton radiation and/or HLU. Panel A: Control; panel B: Combined treatments. eNOS-positive cells were identified with red fluorescence, and endothelia were stained with lectin (green). The nuclei of photoreceptors were counterstained with DAPI (blue). eNOS-positive cells that were located within red lectin-labeled endothelia were identified as eNOS-positive endothelial cells. ONL = outer nuclear layer; INL = inner nuclear layer; GCL = ganglion cell layer. The arrow indicates eNOS-positive endothelial cells. In the nonirradiated retinal tissue, only sparse eNOS-positive cells were found. In the retina of the combined treatments (50 cGy with HLU), eNOS-positive labeling was apparent in the endothelial cells. Scale bar = 50 μm. Red autofluorescence was noted in the outer layers.
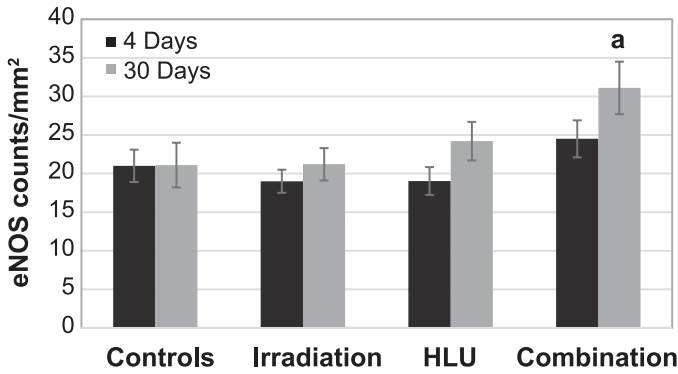
FIG. 5. eNOS immunoreactivity after proton irradiation and/or HLU. Values are represented as mean density of eNOS-positive endothelial cells ± SEM for 8 mice/group. ''a'' indicates significantly higher than control and irradiation-only groups ($P < 0.05$).

effects of radiation ($P < 0.05$) for T- and NK-cell counts in the blood (Fig. 8). The irradiation and combined treatments groups had a higher proportion of NK cells compared to control ($P < 0.05$). There was no effect on B-cell counts at this time point.

By day 30, the proportion of B cells was significantly lower in the irradiation and combined treatments groups compared to controls ($P < 0.05$). Our results showed that there was a strong interaction between radiation exposure and HLU, especially for NK cells, in the blood at both days 4 and 30. Only weak effects were seen for the spleen (data not shown).

DISCUSSION

It is important in risk assessment to determine whether the low-dose radiation response is modulated by simulated microgravity. In this study, we used a ground-based animal
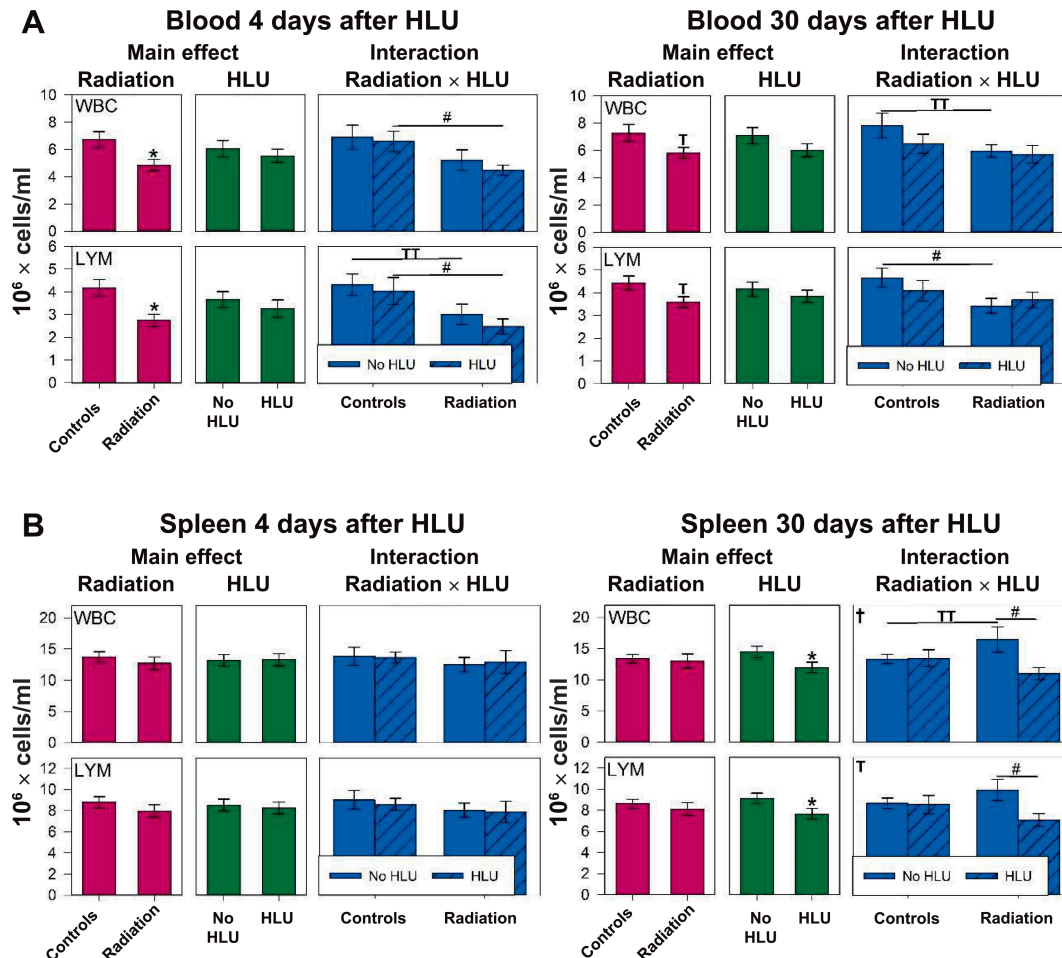
FIG. 6. White blood cell (WBC) and lymphocyte (LYM) counts in the blood (panel A) and spleen (panel B) after irradiation and/or HLU. Mice were euthanized and blood was collected in EDTA-coated syringes via inferior vena cava at day 4 or 30 after unloading (day 11 and 37 postirradiation, respectively). Blood and spleens were analyzed using an automated hematology analyzer. Three-way ANOVA: *$P < 0.05$, main effect of proton radiation or HLU, †$P < 0.05$, irradiation × HLU interaction. $^{T}P < 0.1$, irradiation × HLU interaction. Post hoc Tukey test: #$P < 0.05$, $^{TT}P < 0.1$. Note the strong radiation dependence at day 4 after treatment, but smaller influence of HLU for both WBCs and lymphocytes.
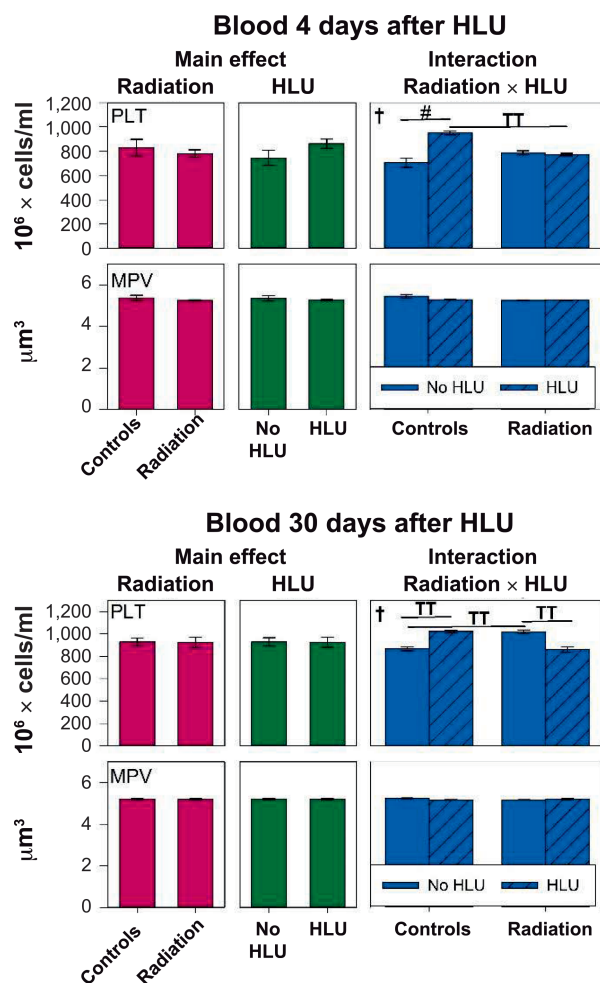
FIG. 7. Platelet (PLT) counts and mean platelet volume (MPV) in the blood after irradiation and/or HLU at day 4 or 30 after HLU (day 11 and 37 postirradiation, respectively). Three-way ANOVA: $^{\dagger}P < 0.05$, irradiation × HLU interaction; $^{T}P < 0.1$, irradiation × HLU interaction. Post hoc Tukey test: $^{\#}P < 0.05$, $^{TT}P < 0.1$. Note the strong HLU dependence at day 4 after treatments, but smaller influence of radiation for PLT counts.

model to assess the biological effects of spaceflight conditions, combining space-like radiation exposure and microgravity. This study design more accurately modeled environmental stressors inherent to the spaceflight environment, providing a more realistic risk assessment for astronauts. To our knowledge, this is the first study to examine the effects of simulated space flight on retinal oxidative damage.

Combined exposure to ionizing radiation and HLU induces cellular and immune response significantly at days 4 and 30 postirradiation. A short latency between exposures to tested stressors and the onset of oxidative changes in retinal endothelial cells and some hematopoietic parameters were observed at day 4 after proton irradiation and HLU. Time points chosen for our study were based on previously published studies, which have reported that exposure to ionizing radiation results in rapid depletion of peripheral
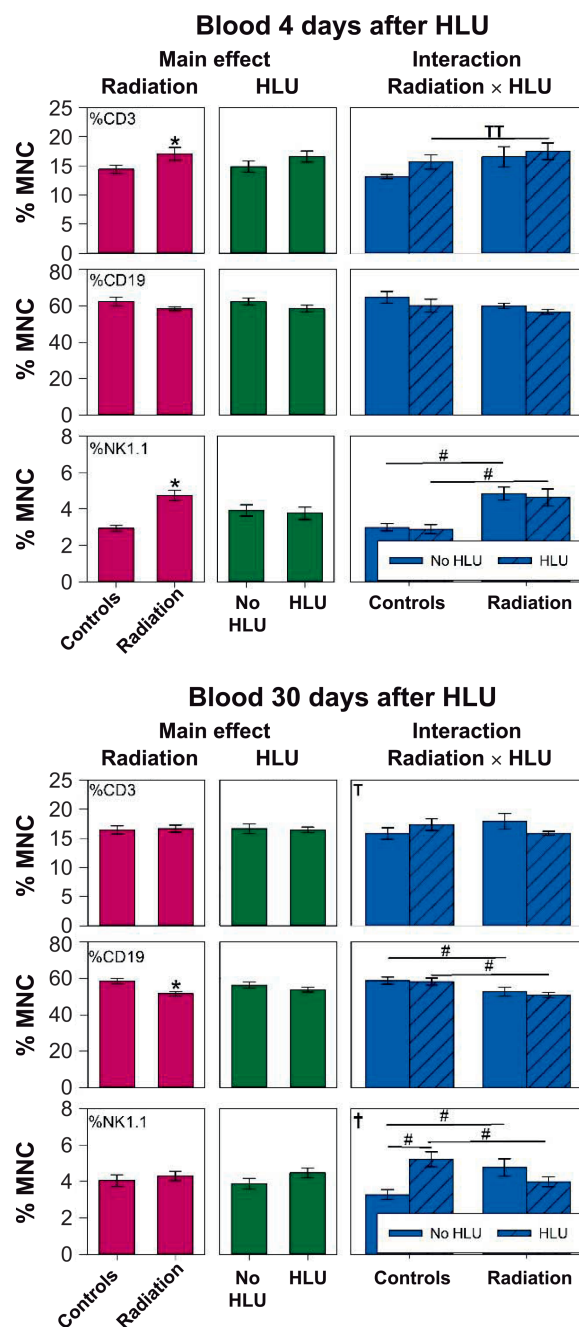
FIG. 8. Major lymphocyte subpopulations in the blood. T (CD3^{+}), B (CD 19^{+}) and NK (NK1.1) cell counts are presented as percentages of all mononuclear cells (MNCs). Data were obtained using fluorescence-labeled monoclonal antibodies and flow cytometry. Mice were euthanized and blood was collected in EDTA-coated syringes via inferior vena cava at day 4 or 30 after HLU (day 11 and 37 postirradiation, respectively). Blood samples were analyzed using flow cytometry. Three-way ANOVA: $^{*}P < 0.05$, main effect of proton radiation or HLU; $^{\dagger}P < 0.05$, irradiation × HLU interaction; $^{T}P < 0.1$, irradiation × HLU interaction. Post hoc Tukey test: $^{\#}P < 0.05$, $^{TT}P < 0.1$.

blood WBCs to a minimum at day 4 postirradiation followed by a restoration by days 14–30 (27, 28).

One of the mechanisms involved in the response to environmental stress including spaceflight and radiation

exposure is acute and chronic oxidative stress (*29*). Persistent upregulation of oxidative stress has been demonstrated in the retina of mice after spaceflight and radiation exposure (*11, 25, 30*), and many of these changes have been implicated in functional consequences including visual impairment (*31, 32*). Similarly, exposure to simulated microgravity also results in enhanced ROS production that may contribute to unloading-induced oxidative stress (*33, 34*). The CNS is sensitive to oxidative injury due to high concentrations of oxidizable, unsaturated lipids and low levels of antioxidant defenses. The retina contains a high level of polyunsaturated fatty acids, making it susceptible to lipid peroxidation (*35*). In many cases, cell death induced by oxidative damage has been identified as occurring via the process of apoptosis (*36*). Oxidative stress has also been implicated in the pathogenesis of many ocular lesions and diseases. A large body of evidence supports that increases in oxidative stress in retinal endothelial cells, and microvasculature is a key factor for the development of retinal vascular diseases (*37–39*). The current study demonstrates that HLU and radiation exposure both induce apoptosis in the mouse retina. There were synergistic effects of HLU and proton radiation on increased apoptosis at the early time point. At the later time point, apoptotic damage due to combined or individual stressors are similar, which may indicate biological regulation of damage response and repair.

Exposure to microgravity induces inflammatory responses and modulates immune functions. Altered immune responses increase ROS production that can promote microgravity-associated oxidative stress (*40*). In-flight data also suggest that oxidative stress is an observed outcome in a long-duration spaceflight (*41*). Our data showed that eNOS expression was significantly increased after combined exposure to simulated space radiation and HLU at day 30, but not significantly altered at day 4. At the early time point, several other potential sources of ROS and factors in neuronal tissues may contribute to cellular response after simulated space radiation or microgravity, including xanthine oxidase, mitochondrial enzymes and enzymes involved in NO synthesis or arachidonic acid metabolism and NADPH oxidase (*42*). In our future work, to determine the extent of oxidative stress in the retina after radiation exposure and unloading, the production of other stress markers will be assessed. The increased number of apoptotic cells found in this study supports the notion that apoptotic mechanisms are involved in retina cell death.

The current study demonstrates the effects of low-dose radiation and simulated microgravity on immune populations. There were significant or strong trend decreases in WBC counts, as well as the lymphocyte population in the blood, but not in the spleen, on days 4 and 30 after proton irradiation. These findings indicate that body compartment (blood versus spleen) may make a difference in leukocyte survival after oxidative stress (*43*). Radiation-induced reduction in leukocyte population counts by day 30

postirradiation were noted, suggesting a relatively long-term radiation effect. Obtained results were consistent with results of previously published studies using larger doses of acutely delivered protons (*44, 45*).

When broad energy spectrum proton radiation at doses of 50 cGy and HLU are used in a combined motif, a synergistic (or additive) effect of radiation dose and HLU is not consistent with many of our measured parameters, and the effects of HLU on hematological assessment appear to be mild for most parameters. Others have also reported that combined treatments (radiation with HLU) did not exacerbate the deleterious effects of SPE-like proton radiation in circulating immune cells (*20*). However, we observed a strong interaction between irradiation and HLU in their effect on the splenic lymphocytes at day 30.

It is also well known that immune cells respond to ionizing radiation with distinct characteristics that depend on the radiation dose and time (*16*). Different cell populations are known to have different sensitivity to radiation. Furthermore, radiation and unloading-induced effects on lymphocytes but not on monocytes/macrophages and granulocytes suggests that survival and/or DNA repair mechanisms in lymphocytes were less efficient after irradiation. The lymphocytes, especially T, B and NK cells, are essential for optimal immune defenses (*46*). Analysis of lymphocyte subpopulations showed that radiation alone, or in combination with HLU, significantly reduced B-cell counts and elevated NK-cell counts in the blood on day 30. This could result in a proportional shift in favor of cell populations involved in innate immunity.

In contrast to leukocytes a dose 50 cGy proton radiation and HLU had little effect on erythrocytes or platelet counts. This may indicate their different response in radiosensitivity, cycling kinetics, DNA repair capacity and other innate characteristics. Hematopoietic progenitors are heterogeneous in their ability to repair damage and repopulate after exposure to ionizing radiation (*47*). Although some of the observed changes in hematopoietic populations were relatively small, it remains to be determined whether these changes will increase over time and whether the findings have a long-term effect on immune function and their ability to maintain homeostasis.

In conclusion, our data show that proton irradiation alone or combined with simulated microgravity has a significant effect on retinal endothelial cell survival and some measured immune parameters based on numerical changes in immune cell populations. Reduction in lymphocytes and WBCs could compromise immune function and increase the risk for developing immune diseases. Future studies will focus on determining the late and long-term effects and functional consequences of observed changes.

REFERENCES

1. Mader TH, Gibson CR, Pass AF, Kramer LA, Lee AG, Fogarty J, et al. Optic disc edema, globe flattening, choroidal folds, and hyperopic shifts observed in astronauts after long-duration space flight. Ophthalmology 2011; 118:2058–69.

2. George K, Rhone J, Beitman A, Cucinotta FA. Cytogenetic damage in the blood lymphocytes of astronauts: effects of repeat long-duration space missions. Mutat Res 2013; 756:165–9.

3. Taibbi G, Cromwell RL, Kapoor KG, Godley BF, Vizzeri G. The effect of microgravity on ocular structures and visual function: a review. Suv Ophthalmol 2013; 58:155–63.

4. Patel N, Pass A, Mason S, Gibson CR, Otto C. Optical coherence tomography analysis of the optic nerve head and surrounding structures in long-duration International Space Station astronauts. JAMA Ophthalmol 2018; 136:193–200.

5. Morgan WH, Balaratnasingam C, Lind CR, Colley S, Kang MH, House PH, et al. Cerebrospinal fluid pressure and the eye. Br J Ophthalmol 2016; 100:71–7.

6. Zhao D, He Z, Vingrys AJ, Bui BV, Nguyen CT. The effect of intraocular and intracranial pressure on retinal structure and function in rats. Physiol Rep. 2015; 3.

7. Liu W, Zhu X, Zhao L, Yang X, Cao F, Huang Y, et al. Effects of simulated weightlessness on biological activity of human NK cells induced by IL-2. 2015; 31:1297–300.

8. Chen Y, Xu C, Wang P, Cai Y, Ma H. Effect of long-term simulated microgravity on immune system and lung tissues in rhesus macaque. Inflammation 2017; 40:589–600.

9. Chancellor JC, Scott GB, Sutton JP. Space Radiation: The number one risk to astronaut health beyond low Earth orbit. Life (Basel) 2014; 4:491–510.

10. Mao XW, Green LM, Mekonnen T, Lindsey N, Gridley DS. Gene expression analysis of oxidative stress and apoptosis in proton-irradiated rat retina. In Vivo 2010; 24:425–30.

11. Mao XW, Pecaut MJ, Stodieck LS, Ferguson VL, Bateman TA, Bouxsein M, et al. Space flight environment induces mitochondrial oxidative damage in ocular tissue. Radiat Res 2013; 180:340–50.

12. Mayer M, Kaiser N, Layer PG, Frohns F. Cell cycle regulation and apoptotic responses of the embryonic chick retina by ionizing radiation. PLoS One 2016; 11:e0155093.

13. Frizziero L, Parrozzani R, Midena G, Miglionico G, Vujosevic S, Pilotto E, et al. Hyperreflective intraretinal spots in radiation macular edema on spectral domain optical coherence tomography. Retina 2016; 36:1664–9.

14. Vinogradova IuV, Tronov VA, Liakhova KN, Poplinskaia VA, Ostrovskii MA. Damage and functional recovery of the mouse retina after exposure to ionizing radiation and methylnitrosourea. Radiats Biol Radioecol 2014; 54:385–92.

15. Gridley DS, Rizvi A, Luo-Owen X, Makinde AY, Coutrakon GB, Koss P, et al. Variable hematopoietic responses to acute photons, protons and simulated solar particle event protons. In Vivo 2008; 22:159–69.

16. Gridley DS, Pecaut MJ, Dutta-Roy R, Nelson GA. Dose and dose rate effects of whole-body proton irradiation on leukocyte populations and lymphoid organs: Part I. Immunol Lett 2002; 80:55–66.

17. Gridley DS, Pecaut MJ. Whole-body irradiation and long term modification of bone marrow-derived cell populations by low- and high-LET radiation. In Vivo 2006; 20:781–9.

18. Kajioka EH, Andres ML, Li J, Mao XW, Moyers MF, Nelson GA, et al. Acute effects of whole-body proton irradiation on the immune system of the mouse. Radiat Res 2000; 153:587–94.

19. Pecaut MJ, Gridley DS and Nelson GA: Long term effects of low dose whole-body proton irradiation on immunity: Shielded vs. unshielded. Aviat Space Environ Med 2003; 74:115–124.

20. Romero-Weaver AL, Lin LY, Carabe-Fernandez A, Kennedy AR. Effects of solar particle event-like proton radiation and/or simulated microgravity on circulating mouse blood cells. Gravit Space Res 2014; 2:42–53.

21. Li M, Holmes V, Zhou Y, Ni H, Sanzari JK, Kennedy AR, Weissman D. Hindlimb suspension and SPE-like radiation impairs clearance of bacterial infections. PLoS One 2014; 9:e85665.

22. Pennathur S, Heinecke JW. Oxidative stress and endothelial dysfunction in vascular disease. Curr Diab Rep 2007; 7.

23. Forstermann U, Munzel T. Endothelial nitric oxide synthase in vascular disease: from marvel to menace. Circulation 2006; 113:1708–14.

24. Rafikov R, Fonseca FV, Kumar S, Pardo D, Darragh C, et al. eNOS activation and NO function: structural motifs responsible for the posttranslational control of endothelial nitric oxide synthase activity. J Endocrinol 2011; 210:271–84.

25. Mao XW, Boerma M, Rodriguez D, Campbell-Beachler M, Jones T, Stanbouly S. Acute effect of low-dose space radiation on mouse retina and retinal endothelial cells. Radiat Res 2018; 190:45–52.

26. Morey-Holton ER, Globus RK. Hindlimb unloading rodent model: technical aspects J Appl Physiol 2002; 92: 1367–77.

27. Pecaut MJ, Gridley DS. The impact of mouse strain on iron ion radio-immune response of leukocyte populations. Int J Radiat Biol 2010; 86:409–19.

28. Wang Y, Chang J, Li X, Pathak R, Sridharan V, Jones T, et al. Low doses of oxygen ion irradiation cause long-term damage to bone marrow hematopoietic progenitor and stem cells in mice. PLoS One 2017; 12:e0189466.

29. Robbin ME, Zhao W. Chronic oxidative stress and radiation-induced late normal tissue injury: a review. Int J Radiat Biol 2004; 80:251–9.

30. Cheng LB, Li KR, Yi N, Li XM, Wang F, Xue B, et al. miRNA-141 attenuates UV-induced oxidative stress via activating Keap1-Nrf2 signaling in human retinal pigment epithelium cells and retinal ganglion cells. Oncotarget 2017; 8:13186–94.

31. Jiang T, Chang Q, Cai J, Fan J, Zhang X, Xu G. Protective effects of melatonin on retinal inflammation and oxidative stress in experimental diabetic retinopathy. Oxid Med Cell Longev 2016:3528274.

32. Berkowitz BA, Kern TS, Bissig D, Patel P, Bhatia A, Kefalov VJ, et al. Systemic retinaldehyde treatment corrects retinal oxidative stress, rod dysfunction, and impaired visual performance in diabetic mice. Invest Ophthalmol Vis Sci 2015; 56:6294–303.

33. Mao XW, Nishiyama NC, Pecaut MJ, Campbell-Beachler M, Gifford P, Haynes KE, et al. Simulated microgravity and low-dose/low-dose-rate radiation induces oxidative damage in the mouse brain. Radiat Res 2016; 185:647–57.

34. Chowdhury P, Soulsby ME, Scott JL. Effects of aminoguanidine on tissue oxidative stress induced by hindlimb unloading in rats. Ann Clin Lab Sci 2009; 39:64–70.

35. Ohie SE, Opere CA, Leday AM. Pharmacological consequences of oxidative stress in ocular tissues. Mutat Res 2005; 579:22–36.

36. Gobbel GT, Bellinzona M, Vogt AR, Gupta N, Fike JR, Chan PH. Response of postmitotic neurons to X-irradiation: implications for the role of DNA damage in neuronal apoptosis. J Neurosci 1998; 18:147–55.

37. Carbajal JM, Schaeffer RC. H2O2 and genistein differentially modulate protein tyrosine phosphorylation, endothelial morphology, and monolayer barrier function. Biochem Biophys Res Commun 1998; 249:461–6.

38. Du Y, Miller CM, Kern TS. Hyperglycemia increases mitochondrial superoxide in retina and retinal cells. Free Radic Biol Med 2003; 35:1491–9.

39. Kowluru RA. Diabetic retinopathy: mitochondrial dysfunction and retinal capillary cell death. Antioxid Redox Signal 2005; 7:1581–7.

40. Wise KC, Manna SK, Yamauchi K, Ramesh V, Wilson BL, Thomas RL, et al. Activation of nuclear transcription factor-kappaB in mouse brain induced by a simulated microgravity environment. In Vitro Cell Dev Biol Anim 2005; 41:118–23.

41. Markin, AA, Zhuravleva OA. Lipid peroxidation and antioxidant defense system in rats after a 14-day space flight in the ''Space-2044'' spacecraft. Aviakosm Ekolog Med 1993; 27:47–50.

42. Faraci FM. Reactive oxygen species: influence on cerebral vascular tone. J Appl Physiol 2006; 100:739–43.

43. Gridley DS, Freeman TL, Makinde AY, Wroe AJ, Luo-Owen X, Tian J, et al. Comparison of proton and electron radiation effects on biological responses in liver, spleen and blood. Int J Radiat Biol 2011; 87:1173–81.

44. Luo-Owen X, Pecaut MJ, Rizvi A, Gridley DS. Low-dose total-body g irradiation modulates immune response to acute proton radiation. Radiat Res 2012; 177:251–64.

45. Gridley DS, Pecaut MJ, Green LM, Sanchez MC, Kadhim MA. Strain-related differences and radiation quality effects on mouse leukocytes: gamma-rays and protons (with and without aluminum shielding). In Vivo 2011; 25:871–80.

46. Gridley DS, Luo-Owen X, Rizvi A, Makinde A, Pecaut M, Mao XW, et al. Low-dose photon and simulated solar particle event proton effects on Foxp3+ T regulatory cells and other leukocytes. Technol Cancer Res Treat 2010; 9:637–49.

47. Wagwemaker G. Heterogeneity of radiation sensitivity of hemopoietic stem cell subsets. Stem Cells 1995; 13: S257–60.